Tracing silicate weathering processes in the permafrost-dominated Lena River watershed using lithium isotopes

Melissa J. Murphy[*a], Don Porcelli[a], Philip A.E. Pogge von Strandmann[b], Catherine A. Hirst[c,d], Liselott Kutscher[c,e], Joachim A. Katchinoff[f], Carl-Magnus Mörth[e], Trofim Maximov[g], Per S. Andersson[c]

a Department of Earth Sciences, University of Oxford, South Parks Road, Oxford OX1 3AN, UK.

b London Geochemistry and Isotope Centre (LOGIC), Institute of Earth and Planetary Sciences, University College London and Birkbeck College, Gower Street, London, WC1E 6BT, UK.

c Department of Geosciences, Swedish Museum of Natural History, Box 50007, SE-104 05 Stockholm, Sweden.

d Earth and Life Institute, Université catholique de Louvain, Croix du Sud, L7.05.10, B-1348 Louvain-la-Neuve, Belgium

e Department of Geological Sciences, Stockholm University, SE-10691 Stockholm, Sweden.

f Department of Geology & Geophysics, Yale University, USA.

g Institute for Biological Problems of the Cryolithozone, Siberian Branch, Russian Academy of Science, Russia.

*Corresponding author: Now at: London Geochemistry and Isotope Centre (LOGIC), Institute of Earth and Planetary Sciences, University College London and Birkbeck College, Gower Street, London, WC1E 6BT, UK. Email address: melissa.murphy@ucl.ac.uk

Abstract

Increasing global temperatures are causing widespread changes in the Arctic, including the thawing of permafrost and the altering freshwater inputs and trace metal and carbon fluxes into the ocean and atmosphere. Strong seasonal changes in the permafrost active layer thickness can affect subsurface water flow-paths and water-rock interaction times, and hence weathering processes. Riverine lithium isotopes (reported as δ^7Li) are tracers of silicate weathering that are seemingly unaffected by biological uptake, redox, carbonate weathering and primary lithology. Here we use Li isotopes to examine silicate weathering processes in the catchment of one of the largest Russian Arctic rivers: the Lena River in eastern Siberia. The Lena River watershed is a large multi-lithological catchment, largely underlain by continuous permafrost. An extensive dataset of dissolved Li isotopic compositions of waters from the Lena River main channel, two main tributaries (the Aldan and Viliui Rivers) and a range of smaller sub-tributaries are presented from the post-spring flood/early-summer period at the onset of active layer development and enhanced water-rock interactions. The Lena River main channel (average δ^7Li_{diss} ~19‰) has a slightly lower isotopic composition than the mean global average of 23‰ (Huh et al., 1998a). The greatest range of [Li] and δ^7Li_{diss} are observed in catchments draining the south-facing slopes of the Verkhoyansk Mountain Range. South-facing slopes in high-latitude, permafrost-dominated regions are typically characterised by increased summer insolation and high daytime temperatures, which contribute to more rapid thawing of snow cover, warmer soils, and repeated freeze/thaw cycles. The greater variability in Li characteristics in these rivers may then partly reflect the greater active layer thaw depth and hence greater infiltration of melt water typical of south-facing slopes in permafrost regions.

A similar magnitude of isotopic fractionation is observed between the contrasting low-lying regions of the Central Siberian Plateau (and catchments draining into the Viliui River), and catchments draining the mountainous regions of the Verkhoyansk Mountain Range into the Aldan River. This is in contrast to global rivers in non-permafrost terrains that drain high elevations or areas of rapid uplift, where high degrees of physical erosion promote dissolution of freshly exposed primary rock typically yields low δ^7Li_{diss}, and low-lying regions exhibit high values resulting from greater water-rock interaction and formation of secondary mineral that fractionates Li isotopes. Overall, the range of Li concentrations and δ^7Li_{diss} observed within the Lena River catchment show a similar range to compositions from global rivers located in temperate and tropical regions. This suggests that cryogenic weathering features specific to permafrost regions (such as the continual

exposure of fresh primary minerals due to seasonal freeze/thaw cycles, frost shattering and salt weathering), and indeed climate (temperature and runoff), are not a dominant control on δ^7Li variations. Despite vastly different climatic and weathering regimes, the same range of riverine δ^7Li values globally suggests that the same processes govern global Li geochemistry – that is, the balance between the dissolution of primary silicate minerals and the formation (or exchange with) secondary minerals. This has implications for the use of δ^7Li as a palaeo-weathering tracer for interpreting changes in past weathering regimes.

1. Introduction

Permafrost thawing in high-latitude polar regions that is induced by climate warming influences mineral, elemental, nutrient and carbon fluxes (dissolved and particulate) into the ocean and atmosphere. Changes in the permafrost active layer thickness dictate subsurface water flowpaths, as well as water-rock interaction times and hence weathering processes, and this may impact future terrestrial biogeochemical cycles (Frey and McClelland, 2009). The evolution of long-term climate is influenced by the supply of cations from silicate weathering (providing alkalinity, which sequesters CO_2 by carbonate precipitation in the oceans), as well as by delivering nutrients that facilitate organic carbon burial (Walker et al., 1981; Berner et al., 1983). To date, however, understanding the influence of climatic (e.g., temperature and runoff) and physical rock supply (e.g., sediment supply, physical erosion) controls on weathering are uncertain and highly debated (e.g., Raymo and Ruddiman, 1992; West et al., 2005; Hilley et al., 2010; Eiriksdottir et al., 2013). Changes in silicate weathering are in turn predicted to have significantly affected long- and short-term climate perturbations in the past (Raymo et al., 1988; Raymo and Ruddiman, 1992; Pogge von Strandmann et al., 2013).

Water-rock interactions, and hence silicate weathering, in cold-climate regions differ from those of warm and wet watersheds in temperate and tropical regions. The latter tend to be characterised by transport- or supply-limited regimes, where weathering rates are limited by the supply of fresh material, with long water-rock interaction times so that minerals are nearly completely altered before their removal and thick soils accumulate (West et al., 2005). In kinetically-limited weathering, the rate of chemical weathering is more limited relative to physical erosion. Soil production is limited because physical erosion removes weathered material more rapidly than it is produced, resulting in shorter water-rock interaction times (Stallard and Edmond, 1983; West et al., 2005).

In high-latitude or alpine regions, low mean annual temperatures are expected to inhibit mineral reaction rates, resulting in incomplete weathering of silicate material (West et al., 2005). Nonetheless, it has been proposed that high rates of physical erosion from frost action and salt weathering, and enhanced primary rock dissolution by organic acids, can promote greater chemical weathering than might otherwise be expected in high-latitude regions dominated by temperature-controlled slow reaction rates (Gislason et al., 1996; Nezat et al., 2001; Huh, 2003).

Most weathering processes observed in weathering regimes in tropical and temperate climates are also prevalent in regions underlain by permafrost. However, the presence of permafrost further complicates water-rock interactions at high altitudes and polar regions. Permafrost underlies nearly a quarter of the northern hemisphere, and underlies approximately 90% of the Lena River catchment, NE Siberia (Brown et al., 1997). Rivers in permafrost-dominated regions have very different hydrologic regimes to rivers in non-permafrost areas. In continuous permafrost-dominated catchments, perennially frozen soil/bed rock inhibits infiltration of surface water, thereby restricting subsurface water storage and limiting water-rock interactions. Rapid melting of winter precipitation (snow) accumulated within the catchment over ~8 to 9 months results in the high runoff spring freshet, which flows over the still frozen permafrost. In early spring, increasing air temperatures promote thawing of the near-surface and development of the 'active layer'. This enables water infiltration into the uppermost shallow (often organic-rich) thawed soil, and water is temporarily stored as ponded surface waters perched above the permafrost in low-lying wetlands and fens. Throughout the summer and early autumn before refreezing occurs, the active layer thaws to its maximum depth, potentially promoting exposure of more readily weathered rocks, deepening of flow paths and allowing greater water interaction with mineral-rich soil horizons (Woo, 2012). Unlike in tropical and temperate regions, the majority of hydrological processes (and hence silicate weathering) in permafrost-dominated terrains occurs within the seasonally thawed active layer (and regions of unfrozen talik) over the short thaw period. Rivers in watersheds with higher permafrost coverage tend to have lower subsurface storage capacity and thus a lower winter base flow and a higher summer peak flow compared to non-permafrost rivers (Woo, 2012; Yang et al., 2009).

In principle, climate warming could drive large annual changes in both the rate of silicate weathering and the weathering regime by contraction of the area underlain by continuous permafrost, increasing active layer thickness, and allowing greater suprapermafrost and talik groundwater flow (Frey and McClelland, 2009). This could affect the biogeochemical cycles of many

elements and the supply of micronutrients to northern oceans. It could also impact the Earth's climate feedback cycles through the release of carbon trapped within permafrost into the atmosphere and oceans. Since the response of weathering processes to permafrost thawing is not well understood (Pokrovsky et al., 2005; Frey et al., 2007; Frey and McClelland, 2009; Keller et al., 2010), it is unknown whether carbon removal via silicate weathering or carbon release from permafrost thawing will have the greatest effect on the carbon budget. Constraining the processes that govern silicate weathering in high-latitude, permafrost dominated regions is therefore critical for quantifying the global carbon cycle over modern and geological timescales.

To date, it has proven difficult to constrain weathering processes at any scale, particularly in permafrost-dominated regions, because most tracers that are used are affected by multiple processes (e.g. biology, lithology, redox, etc.). Riverine lithium isotope ratios ($^{7}Li/^{6}Li$, reported as $\delta^{7}Li$, that is the ‰ deviation from the $^{7}Li/^{6}Li$ ratio of the L-SVEC standard) trace silicate weathering processes at scales ranging from soils and small monolithological catchments to significant global river watersheds that integrate large areas of variable lithology and often several climatic regions. Lithium isotopes are not fractionated in the environment by biological processes (Lemarchand et al., 2007; Pogge von Strandmann et al., 2016). Also, Li is orders of magnitude more concentrated in silicates over carbonates, so that even in carbonate catchments, Li isotopes are dominated by silicate weathering (Kısakűrek et al., 2005; Millot et al., 2010). River $\delta^{7}Li$ values are controlled by what has been described as "silicate weathering congruency" (Misra and Froelich, 2012; Pogge von Strandmann and Henderson, 2015; Vigier and Goddéris, 2015; Pogge von Strandmann et al., 2016; 2017). This is defined as the ratio of primary mineral dissolution (releasing largely unfractionated Li with crustal $\delta^{7}Li$ ~0 to 5‰) to secondary mineral formation (which preferentially incorporate ^{6}Li, increasing the $\delta^{7}Li$ composition of Li remaining in solution; Pistiner and Henderson, 2003; Vigier et al., 2008; Wimpenny et al., 2010a). High riverine $\delta^{7}Li$ values have been interpreted as reflecting less complete weathering, greater secondary mineral formation and thus greater 'weathering intensity' (i.e., the ratio of chemical to physical denudation; Bouchez et al., 2013; Dellinger et al., 2015). There have been a number of large global rivers in tropical and temperate environments where the behaviour of Li isotopes has been studied: e.g., the Amazon River (Chan et al., 1992; Huh et al., 1998a; Dellinger et al., 2014, 2015); the Orinoco River (Huh et al., 1998a; Huh et al., 2001); rivers in the high Himalayas and the Ganges-Brahmaputra (Huh et al., 1998a; Kısakűrek et al., 2005; Bagard et al., 2015; Manaka et al., 2017; Pogge von Strandmann et al., 2017) the Changjiang (Yangtzee) River (Huh et al., 1998a; Liu et al., 2011; Wang et al., 2015); the Mississippi River (Chan et al., 1992;

153 Huh et al., 1998a) and the Congo River (Henchiri et al., 2016). However, there are fewer studies of
154 rivers draining cold climate regions. Whilst some data from Siberia exist, the sampling sites are
155 limited to a handful of locations from the major tributaries and river mouths (Huh et al., 1998a). The
156 only comparable studies of high-latitude polar regions are the Mackenzie River basin (Millot et al.,
157 2010) and the comparatively short rivers of Iceland (Pogge von Strandmann et al., 2006; Vigier et
158 al., 2009; Pogge von Strandmann et al., 2016), Greenland (Wimpenny et al., 2010b), the McMurdo
159 Dry Valleys in Antarctica (Witherow et al., 2010), and Svalbard (Hindshaw et al., 2018).
160 In this study, Li isotopic compositions were measured in over 70 river samples and 11
161 suspended sediments across the catchment of the vast and relatively unstudied Lena River in
162 eastern Siberia. The multi-lithological catchment spans a latitudinal and climate gradient from 60°
163 to 68° N and is largely underlain by continuous permafrost. The effects of secondary mineralogy,
164 climate, topography and presence of permafrost on silicate weathering are investigated. This study
165 vastly increases the amount of Li isotope data from high latitudes, which has been limited partly
166 due to difficulties in logistics and gaining access.
167
168 **2. Background**
169 ***2.1*** *Study Area*
170 The Lena River basin is located in Yakutia in eastern Siberia (Fig. 1). The Lena River is one of
171 the largest Russian Arctic rivers, draining a watershed area of 2.46 x 10^6 km^2. The river flows
172 northwards from 53°N near Lake Baikal to 71°N and enters the Arctic Ocean in the Laptev Sea. The
173 headwaters originate in the discontinuous and patchy mountain permafrost of the Baikal, Stanovoi
174 and Dzhugdzhur mountains. Northward from 60°N latitude, the Lena River watershed is underlain
175 by variable thicknesses of continuous permafrost ranging from 50 meters to over 1500 m (Brown et
176 al., 1997; Chevychelov and Bosikov, 2010). The seasonally thawed active layer varies in thickness
177 throughout the catchment from a few centimetres to several meters (Huh et al., 1998c). The Lena
178 River contributes approximately 15% of the total freshwater input into the Arctic Ocean, of which
179 ~85% is provided during the spring flood and summer months (May – September; Ye et al., 2003).
180 The geology of eastern Siberia has been described in detail by Gordeev and Sidorov, (1993), Huh et
181 al. (1998b, 1998c), and Huh and Edmond, (1999). Briefly, the Central Siberian Plateau (CSP; see Fig.
182 1) is underlain by Proterozoic crystalline and metamorphic basement of the stable Siberian Platform,
183 which outcrop to the south in the mountainous Trans-Baikal region where the headwaters of the
184 Lena River form, and to the east in the Archean Aldan-Stanovoy shield mountains which are drained

by rivers in the Lena-Amginsky inter-river area (LAIRA). The CSP is typified by gentle topography and extensive flood plains, with thick sedimentary cover composed of Precambrian to Quaternary marine carbonates and evaporites, along with terrigenous sandstone, shale, red beds, and coal beds. The Verkhoyansk Mountain Range forms a topographic high to the east, and is composed of folded and metamorphosed rocks and uplifted detrital sediments. It is not actively undergoing tectonic uplift.

The climate of the watershed is continental, characterised by long cold winters and short, hot summers, with temperatures ranging from −50 °C to +35 °C. The mean annual air temperature (MAAT) ranges from −6 to −15°C across the region and decreases with increasing latitude (Fedorov et al., 2014). The mean annual precipitation (MAP) is typically low, ranging from 200 to 500 mm/yr (Chevychelov and Bosikov, 2010). The drainage area is mainly composed of boreal taiga forest of larch and salix in the southern parts of the basin, with exposed rock outcrops, small shrubs, moss and lichen in the tundra regions of the northern part of the basin (Gordeev and Sidorov, 1993).

3. Analytical methods

3.1 Field sampling

The samples and methods are described in detail by Hirst et al. (2017) and Kutscher et al. (2017). Briefly, sampling occurred over two field campaigns (summer of July 2012 and late spring/early summer of June 2013) when the active layer is thickest and so suprapermafrost groundwater flow is deepest. Sampling dates, locations and descriptions are given in Fig. 1 and Table S1. In the field, surface water samples were collected in acid-washed 10 L low density polyethylene (LDPE) bottles by grab sampling from the upstream side of the ship or small motorised boat, or by wading out into river channels. Samples were filtered within a few hours using a polycarbonate Geotech® filter holder and 0.22 µm nitrocellulose filters (Millipore®) prewashed with 5% acetic acid and ultrapure Milli-Q water. At each sampling locality, pH, temperature and electrical conductivity were measured *in-situ* using a multi-meter (YSI 556 multiprobe system) with analytical accuracies of ± 0.03 pH units, ± 0.1 °C, and ± 1 µS/cm.

The rivers for this study have been geographically grouped according to Kutscher et al. (2017): (i) the Lena River main channel; (ii) the low-lying Central Siberian Plateau (CSP) tributaries; (iii) the main channel of the major Viliui River tributary that is sourced from that region; (iv) the mountainous tributaries draining the Verkhoyansk Mountain Range (VMR); (v) the main channel of

the major Aldan River tributary; and (vi) tributaries draining the Lena-Amginsky inter-river area (LAIRA).

3.2 *Major cation and trace element analyses*

Major cations were measured by Inductively Coupled Plasma Optical Emission Spectroscopy (ICP-OES Thermo Icap 6500 Duo) at the Department of Geological Sciences, Stockholm University. For details, see Sun et al. (2018). For the majority of samples, Li concentrations were analysed using an Element 2 sector-field Inductively-Coupled-Plasma Mass Spectrometer (ICP-MS) at the University of Oxford. For Li analyses, standard addition calibration curves were prepared by doping a given sample with a multi-elemental standard solution (Alfa Aesar®) to account for matrix effects. Both standard and water samples were doped with 1 ng/g of rhenium internal standard to correct for instrumental drift. Accuracy was assessed by analysing IAPSO seawater and the international river reference standard SLRS-5, and by measuring samples in duplicate, and external analytical uncertainties were better than 5%. For a handful of samples with Li concentrations below the limit of detection on the Element 2 (<60 nM Li, see Table 1), concentrations were estimated by intensity matching against a known concentration of L-SVEC on the MC-ICP-MS (see below), with uncertainties estimated to be ± 10%.

3.3 *Li isotope measurements*

For Li isotope analysis of the waters, a sufficient volume of each sample was evaporated to yield 10-20 ng Li, and refluxed 1-2 times with concentrated HNO_3 to break down organics prior to separation. This stage is necessary in these organic-rich samples, and resulted in an improvement of internal precision on the measurements by *ca.* 50%. For the suspended sediments, filters were digested using protocols outlined by Hirst et al. (2017). Evaporated water samples and aliquots of the filter digests were dissolved in 0.2 M HCl and passed through a two-stage cation exchange chromatography procedure (BioRad® AG50W-X12), using dilute HCl as an eluent (Pogge von Strandmann et al., 2011; Pogge von Strandmann and Henderson, 2015). In order to confirm that quantitative Li yields on the column were achieved and no significant fractionation occurred on the column, aliquots before and after the main elution were analysed. Blanks for the total chemical procedure were less than 5 pg Li, which is negligible relative to the 10–20 ng of Li analysed in each sample.

Lithium isotope compositions were determined on a Nu Plasma HR-MC-ICP-MS at the Department of Earth Sciences, University of Oxford, in dry plasma mode using a Cetac Aridus-II desolvating system. Corrections for instrumental mass bias were made using sample-standard bracketing. Data are reported in δ^7Li notation, the permil deviation of the measured ^{7}Li/^{6}Li ratio from the L-SVEC standard (NIST SRM 8545; Flesch et al., 1973), where $\delta^7Li = [(^7Li/^6Li_{sample})/ (^7Li/^6Li_{L\text{-}SVEC})\text{-}1] \times 1000$. Each sample was analysed in triplicate during the course of each run. Individual errors are the two standard deviation around the mean of at least two, but typically three, replicate measurements. The external reproducibility was determined by repeat measurements of an internal seawater standard processed through the full chemical procedure, which yielded δ^7Li = 31.3 ± 0.7‰ (2sd; n = 20). Two rock standards were also run, granite JG-2 (δ^7Li = 0.4 ± 0.2‰, n=3) and Wyoming oil shale SGR-1b (δ^7Li = 3.6 ± 0.4‰, n=3), and the results are within uncertainty of other published values (Pogge von Strandmann et al., 2017 and references therein). Replicates of samples processed in duplicate (n = 9 waters, 3 sediments) in different analytical sessions are indistinguishable from one another within analytical error, with the exception of LR2012-37, which shows slightly greater variability (1.5‰; Table 1). Duplicates are plotted as the average of the two measurements.

4. Results

Sample location and field parameter data (from Hirst et al. 2017; Kutscher et al. 2017), dissolved [Na] and [Li] (where square brackets denote concentrations), δ^7Li_{diss} and suspended sediment δ^7Li_{susp} are given in Table 1. Other major elemental data are presented in Sun et al. (2018). Lithium concentrations range from 12 to 1520 nM. This range is similar to that observed from long-term seasonal monitoring of the Lena River at Zhigansk (Fig. 1, [Li] = 115 to 628 nM; Holmes et al., 2018). Dissolved δ^7Li values range between +7.1 and +41.9‰ (Fig. 2). Despite the large range of values, the average δ^7Li_{diss} for the geographical regions vary within only a few permil. Average [Li] and δ^7Li_{diss} compositions are presented as box-and whisker plots in Supplementary Fig. 1. Lithium concentrations within the Lena River main channel (average ~134 nM) are lower than the global mean of 215 nM, and are similar to shield-draining rivers elsewhere (Huh et al., 1998a). The Viliui River as well as the tributaries of the CSP, LAIRA and VMR have higher average [Li] (232 to 338 nM) when compared to the Lena River main channel and Aldan River. The greatest ranges in both [Li] and δ^7Li are observed in rivers draining the Verkhoyansk Mountain Range (VMR), and especially in catchments that predominantly have a south-facing aspect (See Fig. 1 and Table 1). Overall, the data presented here are comparable with the more limited previously published data in the Lena River

279 catchment ([Li] = 40 to 3350 nM; δ^7Li = 19.0 to 29.9‰; Huh et al., 1998a). The furthest downstream
280 sample from this study (LR2013-45, [Li] = 192 nM, δ^7Li = 21.3‰) is indistinguishable to sample UL607
281 from the Lena River outflow ~500 km at Kusur measured previously ([Li] = 220 nM, δ^7Li = 21.5‰;
282 Huh et al., 1998a). Both samples LR2013-45 and UL607 were collected during the early summer
283 months (in June 2013 and July 1995, respectively).
284 Using published monthly discharge and [Li] data from R-ArcticNet (http://www.r-
285 arcticnet.sr.unh.edu/v4.0/index.html), ArcticRIMS (http://rims.unh.edu/data.shtml) and the Arctic
286 Great Rivers Observatory (http://arctic greaterivers.org/data.html), an annual discharge-weighted
287 Li flux into the Arctic Ocean of 1.29×10^8 mol/yr can be calculated. Using a [Li] = 192 nM of our
288 northernmost sample (LR2013-45) and the average annual discharge, we obtain an annual flux of
289 1.03×10^8 mol/yr, which is comparable to the estimate of 1.18×10^8 mol/yr by Huh et al. (1998a). This
290 accounts for approximately 1% of the global riverine Li flux into the ocean.
291 The Li isotopic composition of the Lena River main channel is relatively uniform throughout
292 the catchment (~19 ± 2‰; 1σ), and is several permil lower than the global riverine mean of ~23‰
293 (Huh et al., 1998a), with the exception of one atypical sample with high [Li] and δ^7Li (LR2013-41;
294 δ^7Li = 29.0‰, 396 nM). The ranges of δ^7Li and [Li] measured in this study are similar to those of data
295 from other large global rivers systems elsewhere (e.g., the Mackenzie River, Millot et al., 2010; the
296 Ganges-Brahmaputra, Kısakűrek et al., 2005, Bagard et al., 2015, Pogge von Strandmann et al., 2017;
297 and the Amazon, Dellinger et al., 2015).
298 The rivers in the Lena catchment show a broad negative trend between δ^7Li_{diss} and [Li],
299 although the lack of a simple relationship between δ^7Li and Li concentration for the Lena River main
300 channel and the main catchment regions (Fig. 2) indicates that there are a range of processes
301 controlling the Li concentrations and isotope variations. In particular, the data cannot be adequately
302 explained by simple mixing between two endmembers with different isotopic compositions and
303 weathering regimes, as has been inferred for the Mackenzie River Basin (Millot et al., 2010) and the
304 Congo River (Henchiri et al., 2016). This is not unexpected in such a large complex, multi-lithological
305 drainage region.
306 Four sets of samples were collected from the same locations in both the July 2012 and June
307 2013 field campaigns (Table 1; LR2012-23/LR2013-77 and LR2012-24/LR2013-76 from a tributary
308 draining the VMR; LR2012-03/LR2013-78 from the main channel of the Lena River; and LR2012-
309 22/LR2013-38 from the Aldan River). With the exception of the LR2012-24/LR2013-76 pair of
310 samples, which had similar [Li] , the concentrations of samples collected in 2013 were almost double

311 those of their 2012 counterparts. In all instances, however, the δ^7Li values of the samples from the
312 same locations sampled during both campaigns were within 1-2‰ of one another. This might
313 suggest that despite presumed increases in the thickness of the active layer during the warmer
314 months, there is only limited δ^7Li variation.

315 The suspended sediments have a narrow δ^7Li_{susp} range from +0.4 to +5.1‰ (Supplementary
316 Fig. 2), which broadly overlaps with average continental silicate rock values (UCC, ~ 0.6 ± 0.6‰,
317 Teng et al., 2004; Sauzéat et al., 2015; and basalts ~3 to 5‰, Elliott et al., 2006, Tomascak et al.,
318 2008). The suspended sediments are isotopically heavier than the global mean suspended sediment
319 Li isotopic composition for large global rivers of -1.5 ± 1‰ (1σ; Dellinger et al., 2014) but comparable
320 to δ^7Li_{susp} values for other rivers (e.g., the Mackenzie River, Millot et al. 2010; the Ganges-
321 Brahmaputra; Kısakűrek et al. 2005, Bagard et al. 2015, Pogge von Strandmann et al. 2017; the
322 Dongqu, Weynell et al., 2017); and the Amazon, Dellinger et al., 2014). Variations in δ^7Li have been
323 reported for suspended sediments related to variations in Si/Al (a proxy for grain size) in depth
324 profiles in the Amazon, Mackenzie and Ganges-Brahmaputra Rivers that are the result mineral
325 sorting within the water column (Bouchez et al. 2011, Dellinger et al. 2014, Dellinger et al. 2017).
326 However, only suspended sediments from near-surface waters have been collected in this study,
327 and the use of HF in the filter dissolution protocol in these samples precludes the use of Si/Al as a
328 proxy for grain size.

329 The variation in isotopic offset between δ^7Li_{susp} and δ^7Li_{diss} for the different geographical
330 regions within the Lena River watershed are shown in Supplementary Fig. 3. The range of isotopic
331 fractionation factors ($\Delta^7Li_{susp\text{-}diss} = \delta^7Li_{susp} - \delta^7Li_{diss}$) across the Lena River watershed vary between -
332 12.5 to -22.6 ‰. With the exception of the south-facing VMR sample with $\Delta^7Li_{susp\text{-}diss}$ = -34.3‰, the
333 narrow range of values do not allow for discrimination between the geographical regions. The
334 magnitude of $\Delta^7Li_{susp\text{-}diss}$ observed within the Lena River is comparable to values observed in rivers
335 elsewhere ($\Delta^7Li_{susp\text{-}diss}$ = -6 to -36 ‰; Huh et al., 2001; Kısakűrek et al., 2005; (Pogge von Strandmann
336 et al., 2006; Pogge von Strandmann et al., 2010).
337

338 **5. Discussion**

339 The fractionation of Li isotopes is controlled by water-rock interactions during weathering
340 processes, specifically the balance between release of Li during primary silicate rock dissolution,
341 and the preferential incorporation or adsorption of ^6Li during formation of secondary minerals
342 (Pistiner and Henderson, 2003; Vigier et al., 2008; Wimpenny et al., 2010a). The variations in δ^7Li_{diss}

343 across the Lena River catchment reflect numerous complex processes occurring over the
344 watershed. The lack of detailed observational data on the thermal regime for the individual
345 catchment regions (e.g., active layer thaw depths, local microclimate, snow conditions, vegetation,
346 soil properties, moisture content, lateral drainage, ground ice, etc.; Woo, 2012) complicates the
347 interpretation of these isotopic variations to specific permafrost conditions. Here, we attempt to
348 distinguish the dominant processes controlling Li isotope fractionation over such a large, complex,
349 permafrost-dominated watershed.
350
351 ***5.1*** *Sources of dissolved lithium*
352 Although carbonate weathering is the dominant contributor to total dissolved solids (TDS) in the
353 Lena River catchment (Huh et al., 1998c; Huh et al., 1998b; Huh and Edmond, 1999), it contributes
354 only a small fraction of the dissolved Li due to the low [Li] in carbonates. The possibility of inputs of
355 Li from rainwater, ultimately derived from sea spray and so accompanied by other elements in the
356 same proportions as in seawater, was investigated using the methods of Millot et al. (2010) and
357 Dellinger et al. (2014) and a rainwater [Cl] after Gordeev et al. (1996). The range of measured Li/Cl
358 ratios (1.6×10^{-4} to 7.9×10^{-2}) is much higher than the seawater ratio of 5×10^{-5}, and so a negligible
359 (<5%) proportion of riverine Li originates from precipitation. Thus, the δ^7Li data have not been
360 corrected for these inputs, consistent with the approaches of other riverine studies (e.g. Millot et
361 al., 2010; Bagard et al., 2015; Liu et al., 2015; Pogge von Strandmann et al., 2017).
362 Some of the rivers draining the CSP have elevated [Cl] and [$SO4^-$], which might be derived
363 from weathering of evaporites that are abundant within the catchment region (Gordeev and
364 Sidorov, 1993; Huh et al., 1998c; Yoon, 2010). However, as noted by Yoon (2010), this may also
365 reflect a contribution from high [Cl] and [$SO4^-$] groundwaters. Using the same approach as Dellinger
366 et al. (2014), and assuming evaporites have Li/Na = 3×10^{-5}, a low evaporite contribution has only
367 been identified for a number of CSP (LR2013-50 (3%), LR2013-68 (8%), LR2013-79 (9%), LR2013-72
368 (5%)); and Lena River main channel samples (LR2012-30, LR2012-32 and LR2013-48 (~5%); LR2012-
369 31, LR2012-34 and LR2013-49 (~6%)). Overall therefore, the calculations show that dissolved Li is
370 dominantly derived from the weathering of silicate material.
371
372 **5.2** *Secondary mineralogical controls on Li isotope fractionation - Mineral saturation states*
373 The large range of Li isotope ratios observed in rivers has been proposed to reflect mineral-specific
374 isotope fractionation factors controlled by the precipitation of (or interaction with) different

375 secondary mineral assemblages. This has been attributed to differences in bedrock lithology as well
376 as weathering regime and hence weathering intensity, which control the water chemistry by
377 removing major and trace elements from solution as the various secondary mineral phases
378 precipitate (e.g., Millot et al., 2010; Wimpenny et al., 2010b; Pogge von Strandmann et al., 2006,
379 2010).

380 In order to assess the likelihood and mineralogy of secondary mineral formation in the
381 studied rivers, mineral saturation states were calculated with PHREEQC (Parkhurst and Appelo,
382 1999), using the measured dissolved major cation and anion, Al and Fe concentrations, and *in-situ*
383 pH, alkalinity and temperature data (after Hirst et al. 2017 and Sun et al. 2018).

384 The PHREEQC calculations indicate that in river samples from all of the geographical regions
385 within the Lena River watershed, primary minerals such as quartz, olivine, pyroxene and feldspar
386 are undersaturated and so are likely to be dissolving. In contrast, secondary minerals that are
387 oversaturated (SI >0) in all rivers (and hence are likely to be precipitating) include amorphous and
388 crystalline Fe oxyhydroxides (e.g., goethite, hematite, magnetite), Al oxides (e.g., gibbsite), Mn
389 oxides (e.g., birnessite) and phyllosilicate minerals (e.g., K-mica, kaolinite, pyrophyllite). Smectite
390 clay minerals (Ca- and Na-montmorillonite) and illite are only oversaturated within the Aldan and
391 Lena Rivers (Supplementary Fig. 4). These waters were filtered using a 0.22 µm cutoff, and so the
392 oversaturation of amorphous Fe, Al and Mn oxides might reflect colloidal particles that have passed
393 through the filter. These results are consistent with mineralogical assemblages determined by
394 transmission electron microscopy (TEM) and synchrotron-based scanning transmission X-ray
395 microscopy (STXM) identification of colloidal and suspended particulates for the same samples,
396 which show abundant amorphous Fe(III) ferrihydrite on the sample filters (Hirst et al., 2017), and
397 lesser crystalline goethite and hematite, along with clay minerals. There may also be secondary
398 minerals, such as clays, that are inherited from weathering within the soil profile (Dellinger et al.,
399 2014).

400 Links between Li isotope fractionation and specific secondary mineral saturation indeces
401 have been reported in basaltic terrains (Pogge von Strandmann et al., 2006, 2010), and in glacial
402 rivers draining permafrost in west Greenland (Wimpenny et al., 2010b). In this study, however,
403 there is no correlation between dissolved δ^7Li and any PHREEQC calculated mineral saturation
404 states (Supplementary Fig 3.). This is not unexpected for rivers draining large, multi-lithology
405 catchments, where secondary mineralogy will also vary. Hence, whilst an abundance of amorphous
406 and crystalline Fe oxides were observed in the secondary mineral phases on the filters for the

samples across the geographical regions throughout the Lena River watershed (Hirst et al., 2017), the presence of other secondary minerals (particularly clay minerals) are likely to have contributed to the δ^7Li_{susp} due to the incorporation or sorption of ^6Li.

5.3 *Topographical and catchment area controls on Li isotope fractionation*

Topography and relief can exert a strong influence on weathering. In regions unaffected by permafrost, topographically high regions are typically dominated by relatively high physical erosion with high denudation rates (often related to high uplift rates), and so high rates of exposure of fresh mineral surfaces and minimal water-rock interaction times (e.g., Montgomery and Brandon, 2002). This promotes the weathering of primary rock material and limits secondary mineral precipitation (low weathering intensity), and is expected to result in δ^7Li compositions that approach those of the primary weathering rocks. In contrast, non-permafrost rivers in low-lying regions are expected to have higher δ^7Li values, where greater water-rock interaction times promote the formation of secondary minerals and greater adsorption of Li, driving the riverine δ^7Li towards higher values. This relationship has been suggested from a broad negative correlation between δ^7Li and uplift rate in rivers from New Zealand (Pogge von Strandmann and Henderson, 2015) and in rivers draining higher elevations in the Ganges (Pogge von Strandmann et al., 2017) and the Amazon (Dellinger et al., 2015). This is also supported by generally low δ^7Li observed in rivers in the High Himalayas (Huh et al., 1998a; Kısakűrek et al., 2005).

While uplift rates have not been directly quantified for the regions in this study, the mean gradient of the watershed can be used as a general measure of the overall relief. At low slope angles (<15°), a broad positive linear correlation has been shown between catchment slope angle and long-term erosion rate (Montgomery and Brandon, 2002). For catchments in the CSP, LAIRA and the VMR, the mean watershed gradient was calculated using a GIS-based approach as outlined in Kutscher et al. (2017), dividing the watershed length by its maximum elevation. While a meaningful watershed gradient cannot be estimated for the overall Lena, Aldan and Viliui River catchments, a watershed gradient has been estimated for the upper catchment regions draining in to the Villiui River (LR2013-62; 0.96°) and Aldan River (LR2012-13; 3.44°). Catchments of the low-lying CSP have catchment slope angles ranging from 0.24 to 1.04°. The LAIRA has catchment slope angles ranging from 0.43 to 1.65°, and rivers draining the VMR range from 0.94 to 6.34°. Both [Li] and δ^7Li_{diss} show little relationship with mean watershed gradient (Fig. 3). Despite the *ca.* five degree difference in slope angles between rivers draining the low-lying LAIRA and CSP, and the VMR, there is no clear

439 distinction between rivers draining the mountainous and the low-lying regions, with the entire
440 range of [Li] and δ^7Li_{diss} values spanning the full range of catchment slope angles. In fact, the highest
441 δ^7Li_{diss} values observed in the Lena River watershed are from tributaries with the greatest slope
442 angles draining the Verkhoyansk Mountain Ranges.

443 The lack of a trend between δ^7Li and relief in the Lena River catchment may be due to
444 cryogenic weathering processes prevalent in regions of continuous permafrost e.g., the continual
445 supply of fresh primary minerals due to seasonal freeze/thaw cycles, frost shattering and salt
446 weathering (Woo, 2012), none of which are directly relatived to relief (Goodfellow and
447 Boelhouwers, 2013). Weathering rates can also be enhanced over predicted 'inorganic' weathering
448 rates by organic acid weathering (Huh, 2003), and could also be a factor here.

449 The [Li] and δ^7Li data are plotted against catchment area in Fig. 3. In general, discharge is
450 expected to scale with increasing catchment area (Burgers et al., 2014). Whilst no trends can be
451 seen between [Li] and catchment area (except in south-facing VMR rivers, as discussed below), a
452 broad negative trend can be seen with Li isotope composition, with greater variability observed in
453 smaller catchments, and isotopic compositions that approach the global mean value of ~23‰ with
454 larger catchment areas. This pattern likely reflects the dominance of local processes in smaller
455 catchments, which are homogenised and integrated in rivers draining larger catchments.
456
457 **5.4** *Permafrost and climatic controls on Li isotope variations*

458 Since the Lena River watershed covers a vast area, the effects of climate on the distribution
459 of Li isotopes can be considered. For this study, samples have been collected from a latitudinal and
460 climate gradient from 60° to 68° N, corresponding to mean annual air temperatures (MAAT) of −6
461 to −15°C (Gordeev and Sidorov, 1993). This corresponds to a range of maximum active layer
462 temperatures, and so reaction rates for both dissolution and secondary mineral formation, as well
463 as of depths and lengths of time of active layer thawing. To test the effects of temperature, and
464 hence climate, [Li] and δ^7Li_{diss} are shown plotted against latitude, used as a proxy for MAAT
465 (Supplementary Fig. 5). The Lena River main channel δ^7Li_{diss} values show a weak 5‰ increase from
466 the upper to the lower reaches ($R^2 = 0.47$) along the climate gradient. This progressive downstream
467 increase in δ^7Li_{diss} values observed in the Lena River main channel (Fig. 4a) is also observed in the
468 Ganges (Bagard et al., 2015) and the Changjiang Rivers (Wang et al., 2015). After the confluence of
469 the Viliui River, both Li concentrations and δ^7Li_{diss} in the Lena River main channel increase (Fig. 4).
470 This is unlikely to be simple mixing between the two rivers, because there are no trends between

δ^7Li_{diss} and 1/[Li] (Fig. 2). Equally, anthropogenic influences from cities such as Yakutsk and Zhigansk do not appear to influence [Li] or δ^7Li_{diss}. Thus, the evolution of the Lena River δ^7Li_{diss} value likely reflects Li isotope fractionation due to precipitation or interaction with secondary minerals within the river, or local influences from groundwater or porewaters within permafrost soils.

Overall, there are also no clear trends in [Li] and δ^7Li_{diss} values over a *ca.* nine degree latitude gradient, suggesting that variations in the MAAT, and thus climatic conditions, do not have a dominant influence on variations in δ^7Li in the Lena River catchment. This is consistent with the results for rivers in Iceland (Pogge von Strandmann et al., 2010), rivers from different climatic zones of the Cascade Mountains (Colombia River Basalts; Liu et al., 2015) and the Mackenzie River basin (Millot et al., 2010). Interestingly, the greatest variation in both [Li] and δ^7Li_{diss} are observed in the south-facing slopes draining the VMR. South-facing slopes in permafrost regions are typically characterised by increased summer insolation and higher daily temperatures which contribute to more rapid thawing of snow cover, warmer soils, greater active layer depth and hence greater infiltration of melt water (Woo, 2012; Hindshaw et al., 2018). Repeated freezing and thawing due to earlier snow melt can destabilise the soil cover, such that south-facing slopes are typically prone to greater hillslope instability (Vasiliev, 2009; Goodfellow and Boelhouwers, 2013). This may contribute towards local variations in water flow and hence different water-rock interaction times. The lower δ^7Li_{diss} values observed in the VMR therefore likely reflect catchments dominated by lower intensity of weathering, enhanced dissolution of freshly exposed primary rock due to freeze-thaw processes and little fractionation of Li isotopes dues to reduced secondary mineral precipitation or interaction with secondary minerals within the seasonally thawed active layer (i.e., a weathering-limited regime). In contrast, the much higher δ^7Li_{diss} values might reflect increased adsorption on secondary minerals, or dissolution/reprecipitation cycles due to repeated freeze-thaw cycles that promote greater water-rock interaction, significant secondary mineral formation and therefore greater Li isotope fractionation (i.e., high weathering intensity in a transport-limited regime). However, without detailed knowledge of the thermal regime in the individual catchments, it is difficult to speculate further on these processes. A detailed study of the cryogenic weathering processes occurring within a small, well-constrained river catchment draining continuous permafrost would shed some light on the relative importance of these contrasting processes.

5.5 *Modelled Rayleigh fractionation factors and water residence time - Li/Na*

Li and Na are both monovalent alkali metals that reside in primary silicate minerals, and are readily mobilised into solution during weathering processes. During weathering, it is assumed that Li and Na are released congruently, and the Li/Na ratio is progressively diminished by the incremental removal of Li through interaction with secondary minerals that preferentially remove ^{6}Li, either by adsorption onto the surface, by trapping within the interlayer (in the case of 2:1 clays), or by incorporation into the mineral structure. This in turn increases $\delta^{7}Li$ values and decreases Li/Na values in waters. Values for $\delta^{7}Li_{diss}$ are plotted against Li/Na ratios in Figure 5, where a broad negative correlation between these two parameters is evident and similar to that observed in other river systems (Millot et al., 2010; Bagard et al., 2015; Liu et al., 2015; Wang et al., 2015).

The relationship between Li removal into secondary minerals and associated Li isotope fractionation was investigated using modelling approaches of other studies (Pogge von Strandmann et al., 2010a; 2017; Bouchez et al., 2013; Dellinger et al., 2015; Bagard et al., 2015). One model considers a water that initially has Li/Na and $\delta^{7}Li$ values equal to those of weathering rocks, and then is only progressively depleted by incremental loss of Li (while remaining well-mixed). In this case, the value of $\delta^{7}Li$ will increase as Li/Na decreases according to a Rayleigh distillation relationship that is controlled by the fractionation factor (α) that reflects the preferential removal of ^{6}Li.

$$\delta^{7}Li_{diss} = \delta^{7}Li_{0} + 1000(\alpha-1)\ln(f_{diss}^{Li}) \quad (1)$$

where $\delta^{7}Li_{diss}$ is the Li isotope composition of the dissolved phase and $\delta^{7}Li_{0}$ is the value for Li released into the water, equal to the mean $\delta^{7}Li_{rock}$ of the weathered rocks. The term f_{diss}^{Li} is the fraction of Li remaining in solution, calculated using the equation:

$$f_{diss}^{Li} = \frac{Li/Na_{diss}}{Li/Na_{0}} \quad (2)$$

The fractionation lines represent the calculated compositions of waters subjected to different degrees of Li removal from a single starting Li/Na and $\delta^{7}Li$ composition. A starting isotopic composition ($\delta^{7}Li_{0}$) of 0‰ is used, which is a representative value for the average upper continental crust. Changing $\delta^{7}Li_{0}$ to values of -2 to +5‰ observed in riverine suspended sediments, shales and upper continental crustal rocks and basalts will result in small shifts in the model curves (not shown), although this will not substantially affect the range of fractionation factors needed to explain the range of measured compositions. The bedrock Li/Na ratio (and hence the initial ratio of

Li/Na released into waters), is difficult to constrain for such a large, multi-lithological catchment and undoubtedly varies between sub-catchments and across the watershed. To account for a range of possible end-member values, a Li/Na_0 molar ratio of 0.03, equal to the highest dissolved value found in the Lena catchment area, and a value of 0.1, which is that of the upper continental crust (Taylor and McLennan, 1995) have been adopted in the model calculations. This range of initial Li/Na_0 are depicted by the grey box in Fig. 5.

The range of data within the Lena River catchment cannot be explained by a single isotopic fractionation factor. The majority of data fall within the curves for α values ranging from ~0.997 to 0.990 (Δ^7Li = -3‰ and -10‰). However, a number of outliers (particularly for rivers draining south-facing slopes within the VMR) fall outside these α values, requiring a wider range of fractionation factors. The range of isotopic fractionation factors in Fig. 5 are consistent with experimentally determined values for various secondary minerals, including those predicted to be oversaturated within the Lena River (see section 5.2), with $\alpha_{vermiculite}$ = 0.971, $\alpha_{kaolinite}$ = 0.979, $\alpha_{gibbsite}$ = 0.984-0.993, $\alpha_{ferrihydrite}$ ≈ 0.998, and $\alpha_{smectite}$ = 0.984 (Zhang et al. 1998; Pistiner and Henderson, 2003; Millot and Girard, 2007; Vigier et al. 2008; Wimpenny et al. 2015). The range of α is also comparable to that those observed in other global rivers (e.g., Amazon (Dellinger et al., 2015); Ganges (Bagard et al., 2015; Pogge von Strandmann et al., 2017)). Overall, the range of fractionation factors required to explain the data reflects the complex behavior of Li in such a vast catchment. Variations are also expected from other processes, such as mixing between waters with different Li characteristics. In addition, variability may be caused by the uptake of Na into some secondary minerals (such as clays or zeolites), and/or desorption of Na from mineral surfaces in soils, thus decoupling Li/Na from δ^7Li. It is not possible to distinguish whether these processes occur within the river, or is controlled by sub-surface residence time. It is likely that there are also other processes that have caused variations in Li/Na or δ^7Li values, including mixing of porewaters within soils or groundwaters, as well as small scale variations in δ^7Li and Li/Na values. Other interactions, including adsorption, precipitation in other phases, or interaction with organics, may also affect Li concentrations and possibly create further isotope fractionation.

5.6 *Comparison with global rivers*

Huh et al. (1998a) also measured dissolved δ^7Li in the Lena River catchment, and several other Siberian rivers. They observed a wide range in δ^7Li values (~6 to 30‰), similar to the values observed in this study. The dissolved δ^7Li observed in the Lena River catchment (from this study

565 and Huh et al. 1998a) overlap with those of other polar, cold climate rivers that are underlain by
566 continuous, discontinuous, sporadic or isolated permafrost (e.g., the Mackenzie River basin (~9 to
567 29‰; Millot et al., 2010), Spitzbergen (~8 to 14‰; Hindshaw et al., 2018) and Antarctic rivers (~12
568 to 23‰; Witherow et al., 2010)). They also overlap with values from glaciated and non-glaciated
569 rivers in west Greenland that are underlain by permafrost (~14 to 36‰; Wimpenny et al., 2010b),
570 and those of rivers in Iceland that are unaffected by permafrost (~10 to 44‰; Pogge von
571 Strandmann et al., 2006; Vigier et al., 2009).
572 Interestingly, the overall range in δ^7Li and Li/Na values in these cold climate, polar regions
573 (including regions impacted by permafrost and glacial weathering processes) are similar to those
574 found in temperate and tropical rivers (Fig. 6). It has been proposed that weathering rates are
575 strongly controlled by temperature and hence climate (precipitation and runoff) (e.g. West et al.,
576 2005; Gislason et al., 2009). Warmer, wetter watersheds are expected to have greater chemical
577 weathering rates than watersheds in high latitude permafrost-dominated regions, where the cold
578 climate and restricted water-rock and water-soil interactions are predicted to reduce the extent of
579 chemical weathering (Huh and Edmond, 1999). Whilst Li isotopes cannot constrain the rates of
580 silicate weathering (for a discussion, see Pogge von Strandmann et al., 2017), the magnitude of Li
581 isotope fractionation, and hence intensity of weathering (i.e., the rate of secondary mineral
582 formation relative to the rate of primary mineral dissolution) observed in such cold climate, polar
583 regions is partly due to the increased supply of Li from primary minerals due to enhanced physical
584 erosion facilitating greater chemical weathering. The unique role of cryogenic weathering
585 processes such as repeat freeze-thaw cycles, frost shattering and salt weathering continually
586 expose fresh primary minerals and prevents the accumulation of weathered products and
587 development of thick soil profiles. The high degree of physical erosion, together with enhanced
588 chemical weathering by the presence of organic acids is sufficient to overcome the temperature
589 inhibition on the mineral reaction kinetics (Huh et al., 1998b,c; Huh and Edmond, 1999; Woo, 2012).
590 Global rivers are further compared in Figure 7, which shows the frequency of dissolved Li
591 isotope data for some of the large global rivers and rivers draining basaltic terrains. Typically, the
592 Ganges, Lena and basalts all have similar frequency peaks, clustering around the global riverine
593 mean of ~23‰ (Huh et al., 1998a). Rivers draining the high Himalayas have a slightly lower average
594 value (~14 to 16‰), consistent with greater exposure rates of fresh rock driving the Li isotopic
595 compositions towards crustal rock values. Interestingly, the Amazon and Mackenzie Rivers have the
596 lightest mean values of these large datasets, of ~16‰. Hence, the mean values of these different

catchments are quite similar relative to the overall variability in δ^7Li observed in rivers. This, in combination with the trends with Li/Na, further supports the conclusion that climatic controls (e.g., temperature and runoff) are weak secondary controls on Li isotopes and hence silicate weathering processes of primary rock dissolution relative to secondary mineral formation. The data therefore suggest that similar processes control global Li geochemistry in rivers from cold, temperate and tropical regions.

This has implications for the use of δ^7Li as a palaeo-weathering tracer, because it implies that the global riverine mean of 23‰ is not the result of mixing Li with a wide range of δ^7Li values in different rivers (as it is, for example, for $^{87}Sr/^{86}Sr$; Palmer and Edmond, 1989), but rather that many major rivers share a value of ~23‰, irrespective of climate and weathering regime. This therefore suggests that in order to explain the $\delta^7Li_{seawater}$ ~9‰ increase observed during the early Cenozoic (Hathorne and James, 2006; Misra and Froelich, 2012), the global weathering conditions would have to have significantly changed from low weathering intensity conditions imparting low riverine δ^7Li_{diss} input to the oceans, to the present day weathering conditions imparting a mean riverine δ^7Li_{diss} of 23‰. Hence, if the global riverine δ^7Li is not principally controlled by climate, this may suggest that the Cenozoic Li curve may be more significantly controlled by changing riverine fluxes, rather than isotope ratios, possibly coupled with changes associated with the removal of Li from the oceans (Li and West, 2014; Coogan et al., 2017).

6. Conclusions

In this study, we report Li data for over 70 river waters and 11 suspended sediments from the Lena River Basin, a large, complex, multi-lithological catchment underlain by continuous permafrost discharging into the Arctic Ocean. A fractionation factor (α) during weathering of between ~ 0.997 and 0.990 can explain the data for the Lena River, comparable to previously published experimental and field based values from highly disparate climates and weathering regimes. Contrary to reports from other studies from rivers in non-permafrost terrains, there are no systematic trends observed between riverine δ^7L_{diss} and watershed mean slope angle (a proxy for erosion rate), and so between values for rivers draining the Verkhyansk Mountain Range (VMR) when compared to those for low-lying rivers of the Central Siberian Plateau. South-facing catchments from the VMR do exhibit more δ^7Li variation than other areas, likely due to the higher insolation affecting the size of the active layer. Overall, cryogenic weathering processes found in permafrost-dominated regions seasonally likely provide a fresh supply of unweathered primary silicate rock material (due to freeze-thaw

processes), which would lower dissolved δ^7Li. Combined with organic acids that enhance chemical weathering (despite low temperatures hindering weathering rates) and promote secondary mineral formation. Together, these weathering features prevalent within regions of continuous permafrost may obscure any topographical controls on Li isotope fractionation observed in rivers draining non-permafrost.

At the basin scale, the Lena River has a remarkably similar range in δ^7Li values to global rivers from contrasting climate and weathering regimes from polar, temperate and tropical regions. Overall, temperature, the presence of permafrost, and indeed climate are weak controls on riverine Li isotope compositions, and similar processes (that is, the balance between primary silicate mineral dissolution and the preferential incorporation or adsorption of ^{6}Li during formation of secondary minerals) that operate in different climates control global riverine Li geochemistry. This suggests that climate changes likely will little affect the isotope composition of Li delivered to the ocean, and changing riverine flux must be considered when using sedimentary records of Li isotopes to understand changes in past weathering regimes (e.g. Pogge von Strandmann et al., 2017b).

Acknowledgements

This project was funded by the Swedish Research Council (VR 621-2010-3917), the Swedish Polar Research Secretariat (SIMO 2011-165 and 2012-213) and MetTrans, an EU FP7 Marie Curie Initial Training Network grant. We would like to thank Phil Holdship for his assistance with trace element analysis, Yu-Te (Alan) Hsieh for help with the MC-ICP-MS and Jon Wade for assistance with data presentation. We also thank Fang-Zhen Teng (associate editor), Josh Wimpenny, and two anonymous reviewers for constructive comments on an earlier version of the manuscript. PPvS and MJM are supported by ERC Consolidator grant 682760 - CONTROLPASTCO2.

References

Bagard M.-L., West A. J., Newman K. and Basu A. R. (2015) Lithium isotope fractionation in the Ganges–Brahmaputra floodplain and implications for groundwater impact on seawater isotopic composition. *Earth Planet. Sci. Lett.* **432**, 404–414.

Berner R. A., Lasaga A. C. and Garrels R. M. (1983) The carbonate-silicate geochemical cycle and its effect on atmospheric carbon dioxide over the past 100 million years. *Am. J. Sci.* **283**, 641–683.

Bouchez J., von Blanckenburg F. and Schuessler J. A. (2013) Modeling novel stable isotope ratios in the weathering zone. *Am. J. Sci.* **313**, 267–308.

663 Bouchez J., Gaillardet J., France-Lanord C., Maurice L. and Dutra-Maia P. (2011) Grain size control
664 of river suspended sediment geochemistry: Clues from Amazon River depth profiles.
665 *Geochemistry, Geophys. Geosystems* **12**.
666 Burgers H. E. (Robin), Schipper A. M. and Jan Hendriks A. (2014) Size relationships of water
667 discharge in rivers: scaling of discharge with catchment area, main-stem length and
668 precipitation. *Hydrol. Process.* **28**, 5769–5775.
669 Chan L. H., Edmond J. M., Thompson G. and Gillis K. (1992) Lithium isotopic composition of
670 submarine basalts: implications for the lithium cycle in the oceans. *Earth Planet. Sci. Lett.* **108**,
671 151–160.
672 Chevychelov A. P. and Bosikov N. P. (2010) Natural Conditions BT - The Far North: Plant
673 Biodiversity and Ecology of Yakutia. In (eds. E. I. Troeva, A. P. Isaev, M. M. Cherosov, and N. S.
674 Karpov). Springer Netherlands, Dordrecht. pp. 1–23.
675 Coogan L. A., Gillis K. M., Pope M. and Spence J. (2017) The role of low-temperature (off-axis)
676 alteration of the oceanic crust in the global Li-cycle: Insights from the Troodos ophiolite.
677 *Geochim. Cosmochim. Acta* **203**, 201–215.
678 Dellinger M., Bouchez J., Gaillardet J., Faure L. and Moureau J. (2017) Tracing weathering regimes
679 using the lithium isotope composition of detrital sediments. *Geol.* **45**, 411–414.
680 Dellinger M., Gaillardet J., Bouchez J., Calmels D., Galy V., Hilton R. G., Louvat P. and France-Lanord
681 C. (2014) Lithium isotopes in large rivers reveal the cannibalistic nature of modern
682 continental weathering and erosion. *Earth Planet. Sci. Lett.* **401**, 359–372.
683 Dellinger M., Gaillardet J., Bouchez J., Calmels D., Louvat P., Dosseto A., Gorge C., Alanoca L. and
684 Maurice L. (2015) Riverine Li isotope fractionation in the Amazon River basin controlled by
685 the weathering regimes. *Geochim. Cosmochim. Acta* **164**, 71–93.
686 Eiriksdottir E. S., Gislason S. R. and Oelkers E. H. (2013) Does temperature or runoff control the
687 feedback between chemical denudation and climate? Insights from NE Iceland. *Geochim.
688 Cosmochim. Acta* **107**, 65–81.
689 Elliott T., Thomas A., Jeffcoate A. and Niu Y. (2006) Lithium isotope evidence for subduction-
690 enriched mantle in the source of mid-ocean-ridge basalts. *Nature* **443**, 565–568.
691 Fedorov A. N., Ivanova R. N., Park H., Hiyama T. and Iijima Y. (2014) Recent air temperature
692 changes in the permafrost landscapes of northeastern Eurasia. *Polar Sci.* **8**, 114–128.
693 Flesch G. D., Anderson A. R. and Svec H. J. (1973) A secondary isotopic standard for 6Li/7Li
694 determinations. *Int. J. Mass Spectrom. Ion Phys.* **12**, 265–272.
695 Frey K. E. and McClelland J. W. (2009) Impacts of permafrost degradation on arctic river
696 biogeochemistry. *Hydrol. Process.* **23**, 169–182.
697 Frings P. J., Clymans W., Fontorbe G., Gray W., Chakrapani G. J., Conley D. J. and De La Rocha C.
698 (2015) Silicate weathering in the Ganges alluvial plain. *Earth Planet. Sci. Lett.* **427**, 136–148.
699 Frings P. J., Clymans W., Fontorbe G., Rocha C. L. D. La and Conley D. J. (2016) The continental Si
700 cycle and its impact on the ocean Si isotope budget. *Chem. Geol.* **425**, 12–36.
701 Georg R. B., Reynolds B. C., West A. J., Burton K. W. and Halliday A. N. (2007) Silicon isotope
702 variations accompanying basalt weathering in Iceland. *Earth Planet. Sci. Lett.* **261**, 476–490.
703 Georg R. B., West A. J., Basu A. R. and Halliday A. N. (2009) Silicon fluxes and isotope composition
704 of direct groundwater discharge into the Bay of Bengal and the effect on the global ocean
705 silicon isotope budget. *Earth Planet. Sci. Lett.* **283**, 67–74.
706 Gislason S. R., Arnorsson S. and Armannsson H. (1996) Chemical weathering of basalt in Southwest
707 Iceland; effects of runoff, age of rocks and vegetative/glacial cover. *Am. J. Sci.* **296**, 837–907.
708 Goodfellow B. W. and Boelhouwers J. (2013) 7.31 Hillslope Processes in Cold Environments: An
709 Illustration of High-Latitude Mountain and Hillslope Processes and Forms. In *Treatise on*

Geomorphology (ed. J. F. Shroder). Academic Press, San Diego. pp. 320–336.
Gordeev V. V, Martin J. M., Sidorov I. S. and Sidorova M. V (1996) A reassessment of the Eurasian river input of water, sediment, major elements, and nutrients to the Arctic Ocean. *Am. J. Sci.* **296**, 664–691.
Gordeev V. V and Sidorov I. S. (1993) Concentrations of major elements and their outflow into the Laptev Sea by the Lena River. *Mar. Chem.* **43**, 33–45.
Hathorne E. C. and James R. H. (2006) Temporal record of lithium in seawater: A tracer for silicate weathering? *Earth Planet. Sci. Lett.* **246**, 393–406.
Henchiri S., Gaillardet J., Dellinger M., Bouchez J. and Spencer R. G. M. (2016) Temporal variations of riverine dissolved lithium isotopic signatures unveil contrasting weathering regimes in low-relief Central Africa. *Geophys. Res. Lett.* **43**.
Hilley G. E., Chamberlain C. P., Moon S., Porder S. and Willett S. D. (2010) Competition between erosion and reaction kinetics in controlling silicate-weathering rates., *Earth Planet. Sci. Lett.* **293**, 191–199.
Hirst C., Andersson P. S., Shaw S., Burke I. T., Kutscher L., Murphy M. J., Maximov T., Pokrovsky O. S., Mörth C.-M. and Porcelli D. (2017) Characterisation of Fe-bearing particles and colloids in the Lena River basin, NE Russia. *Geochim. Cosmochim. Acta* **213**, 553–573.
Holmes R. M., McClelland J. W., Tank S. E., Spencer R. G. M. and Shiklomanov A. I. (2018) Arctic Great Rivers Observatory. Water Quality Dataset Version 20180321. Available at: https://www.arcticgreatrivers.org/data.
Huh Y. (2003) Chemical weathering and climate --- a global experiment: A review. *Geosci. J.* **7**, 277–288.
Huh Y., Chan L.-H. and Edmond J. M. (2001) Lithium isotopes as a probe of weathering processes: Orinoco River. *Earth Planet. Sci. Lett.* **194**, 189–199.
Huh Y., Chan L.-H., Zhang L. and Edmond J. M. (1998a) Lithium and its isotopes in major world rivers: implications for weathering and the oceanic budget. *Geochim. Cosmochim. Acta* **62**, 2039–2051.
Huh Y. and Edmond J. M. (1999) The fluvial geochemistry of the rivers of Eastern Siberia: III. Tributaries of the Lena and Anabar draining the basement terrain of the Siberian Craton and the Trans-Baikal Highlands. *Geochim. Cosmochim. Acta* **63**, 967–987.
Huh Y., Panteleyev G., Babich D., Zaitsev A. and Edmond J. M. (1998b) The fluvial geochemistry of the rivers of Eastern Siberia: II. Tributaries of the Lena, Omoloy, Yana, Indigirka, Kolyma, and Anadyr draining the collisional/accretionary zone of the Verkhoyansk and Cherskiy ranges. *Geochim. Cosmochim. Acta* **62**, 2053–2075.
Huh Y., Tsoi M.-Y., Zaitsev A. and Edmond J. M. (1998c) The fluvial geochemistry of the rivers of Eastern Siberia: I. tributaries of the Lena River draining the sedimentary platform of the Siberian Craton. *Geochim. Cosmochim. Acta* **62**, 1657–1676.
Kısakűrek B., James R. H. and Harris N. B. W. (2005) Li and δ7Li in Himalayan rivers: Proxies for silicate weathering? *Earth Planet. Sci. Lett.* **237**, 387–401.
Kutscher L., Mörth C.-M., Porcelli D., Hirst C., Maximov T. C., Petrov R. E. and Andersson P. S. (2017) Spatial variation in concentration and sources of organic carbon in the Lena River, Siberia. *J. Geophys. Res. Biogeosciences* **122**, 1999–2016.
Lemarchand E., Schott J. and Gaillardet J. (2007) How surface complexes impact boron isotope fractionation: Evidence from Fe and Mn oxides sorption experiments. *Earth Planet. Sci. Lett.* **260**, 277–296.
Li G. and West A. J. (2014) Evolution of Cenozoic seawater lithium isotopes: Coupling of global denudation regime and shifting seawater sinks. *Earth Planet. Sci. Lett.* **401**, 284–293.

Available at: http://www.sciencedirect.com/science/article/pii/S0012821X14003884.
Liu C.-Q., Zhao Z.-Q., Wang Q. and Gao B. (2011) Isotope compositions of dissolved lithium in the rivers Jinshajiang, Lancangjiang, and Nujiang: Implications for weathering in Qinghai-Tibet Plateau. *Appl. Geochemistry* **26**, S357–S359.
Liu X.-M., Wanner C., Rudnick R. L. and McDonough W. F. (2015) Processes controlling δ7Li in rivers illuminated by study of streams and groundwaters draining basalts. *Earth Planet. Sci. Lett.* **409**, 212–224.
Manaka T., Araoka D., Yoshimura T., Hossain H. M. Z., Nishio Y., Suzuki A. and Kawahata H. (2017) Downstream and seasonal changes of lithium isotope ratios in the Ganges-Brahmaputra river system. *Geochemistry, Geophys. Geosystems* **18**, 3003–3015.
Millot R., Gaillardet J. érôme, Dupré B. and Allègre C. J. (2003) Northern latitude chemical weathering rates: clues from the Mackenzie River Basin, Canada. *Geochim. Cosmochim. Acta* **67**, 1305–1329.
Millot R. and Girard J. P. (2007) Lithium Isotope Fractionation during adsorption onto mineral surfaces. In *Clays in natural & engineered barriers for radioactive waste confinement. 3rd International meeting* Lille, France.
Millot R., Vigier N. and Gaillardet J. (2010) Behaviour of lithium and its isotopes during weathering in the Mackenzie Basin, Canada. *Geochim. Cosmochim. Acta* **74**, 3897–3912.
Misra S. and Froelich P. N. (2012) Lithium Isotope History of Cenozoic Seawater: Changes in Silicate Weathering and Reverse Weathering. *Science (80-.).* **335**, 818–823.
Montgomery D. R. and Brandon M. T. (2002) Topographic controls on erosion rates in tectonically active mountain ranges. *Earth Planet. Sci. Lett.* **201**, 481–489.
Nezat C. A., Lyons W. B. and Welch K. A. (2001) Chemical weathering in streams of a polar desert (Taylor Valley, Antarctica). *Geol. Soc. Am. Bull.* **113**, 1401–1408.
Opfergelt S., Burton K. W., Pogge von Strandmann P. A. E., Gislason S. R. and Halliday A. N. (2013) Riverine silicon isotope variations in glaciated basaltic terrains: Implications for the Si delivery to the ocean over glacial–interglacial intervals. *Earth Planet. Sci. Lett.* **369**–**370**, 211–219.
Palmer M. R. and Edmond J. M. (1989) The strontium isotope budget of the modern ocean. *Earth Planet. Sci. Lett.* **92**, 11–26.
Parkhurst D. L. and Appelo C. A. J. (1999) *User's guide to PHREEQC (Version 2): a computer program for speciation, batch-reaction, one-dimensional transport, and inverse geochemical calculations*.,
Pistiner J. S. and Henderson G. M. (2003) Lithium-isotope fractionation during continental weathering processes. *Earth Planet. Sci. Lett.* **214**, 327–339.
Pogge von Strandmann P. A. E., Burton K. W., James R. H., van Calsteren P. and Gislason, S. R. (2010a) Assessing the role of climate on uranium and lithium isotope behaviour in rivers draining a basaltic terrain. *Chem. Geol.* **270**, 227–239.
Pogge von Strandmann P. A. E., Burton K. W., James R. H., van Calsteren P., Gíslason S. R. and Mokadem F. (2006) Riverine behaviour of uranium and lithium isotopes in an actively glaciated basaltic terrain. *Earth Planet. Sci. Lett.* **251**, 134–147.
Pogge von Strandmann P. A. E., Burton K. W., Opfergelt S., Eiríksdóttir E. S., Murphy M. J., Einarsson A. and Gislason S. R. (2016) The effect of hydrothermal spring weathering processes and primary productivity on lithium isotopes: Lake Myvatn, Iceland. *Chem. Geol.*
Pogge von Strandmann P. A. E., Elliott T., Marschall H. R., Coath C., Lai Y.-J., Jeffcoate A. B. and Ionov D. A. (2011) Variations of Li and Mg isotope ratios in bulk chondrites and mantle xenoliths. *Geochim. Cosmochim. Acta* **75**, 5247–5268.
Pogge von Strandmann P. A. E., Frings P. J. and Murphy M. J. (2017) Lithium isotope behaviour

during weathering in the Ganges Alluvial Plain. *Geochim. Cosmochim. Acta* **198**, 17–31.
Pogge von Strandmann P. A. E. and Henderson G. M. (2015) The Li isotope response to mountain uplift. *Geology* **43**, 67–70.
Pogge von Strandmann P. A. E., James R. H., van Calsteren P. and Gislason S. R. (2010b) Assessing the role of climate on uranium and lithium isotope behaviour in rivers draining a basaltic terrain. *Chem. Geol.* **270**, 227–239.
Pogge von Strandmann P. A. E., Jenkyns H. C. and Woodfine R. G. (2013) Lithium isotope evidence for enhanced weathering during Oceanic Anoxic Event 2. *Nat. Geosci* **6**, 668–672.
Pokrovsky O. S., Schott J., Kudryavtzev D. I. and Dupré B. (2005) Basalt weathering in Central Siberia under permafrost conditions. *Geochim. Cosmochim. Acta* **69**, 5659–5680.
Raymo M. E. and Ruddiman W. F. (1992) Tectonic forcing of late Cenozoic climate. *Nature* **359**, 117–122.
Raymo M. E., Ruddiman W. F. and Froelich P. N. (1988) Influence of late Cenozoic mountain building on ocean geochemical cycles. *Geol.* **16**, 649–653.
Sauzéat L., Rudnick R. L., Chauvel C., Garçon M. and Tang M. (2015) New perspectives on the Li isotopic composition of the upper continental crust and its weathering signature. *Earth Planet. Sci. Lett.* **428**, 181–192.
Stallard R. F. and Edmond J. M. (1983) Geochemistry of the Amazon: 2. The influence of geology and weathering environment on the dissolved load. *J. Geophys. Res. Ocean.* **88**, 9671–9688.
Stefánsson A., Gíslason S. R. and Arnórsson S. (2001) Dissolution of primary minerals in natural waters: II. Mineral saturation state. *Chem. Geol.* **172**, 251–276.
Sun X., Mörth C.-M., Porcelli D., Kutscher L., Hirst C., Murphy M. J., Maximov T., Petrov R. E., Humborg C., Schmitt M. and Andersson P. S. Stable Silicon Isotopic Compositions of the Lena River and its Tributaries: Implications for Silicon Delivery to the Arctic Ocean. *Geochim. Cosmochim. Acta*.
Taylor S. R. and McLennan S. M. (1995) The geochemical evolution of the continental crust. *Rev. Geophys.* **33**, 241–265.
Teng F.-Z., McDonough W. F., Rudnick R. L., Dalpé C., Tomascak P. B., Chappell B. W. and Gao S. (2004) Lithium isotopic composition and concentration of the upper continental crust. *Geochim. Cosmochim. Acta* **68**, 4167–4178.
Tomascak P. B., Langmuir C. H., le Roux P. J. and Shirey S. B. (2008) Lithium isotopes in global mid-ocean ridge basalts. *Geochim. Cosmochim. Acta* **72**, 1626–1637.
Vasiliev I. S. (2009) Mountain permafrost landscapes of Yakutia. *Geogr. Nat. Resour.* **30**, 92–95.
Viers, J., Prokushkin, A.S., Pokrovsky, O.S., Auda, Y., Kirdyanov, A.D., Beaulieu, E., Zouiten, C., Oliva, P., Dupré, B., (2012) Seasonal and spatial variability of elemental concentrations in boreal forest larch foliage of Central Siberia on continuous permafrost. Biogeochemistry xx(xx), pp-pp.
Vigier N., Decarreau A., Millot R., Carignan J., Petit S. and France-Lanord C. (2008) Quantifying Li isotope fractionation during smectite formation and implications for the Li cycle. *Geochim. Cosmochim. Acta* **72**, 780–792.
Vigier N., Gislason S. R., Burton K. W., Millot R. and Mokadem F. (2009) The relationship between riverine lithium isotope composition and silicate weathering rates in Iceland. *Earth Planet. Sci. Lett.* **287**, 434–441.
Vigier N. and Goddéris Y. (2015) A new approach for modeling Cenozoic oceanic lithium isotope paleo-variations: the key role of climate. *Clim. Past* **11**, 635–645.
Walker J. C. G., Hays P. B. and Kasting J. F. (1981) A negative feedback mechanism for the long-term stabilization of Earth's surface temperature. *J. Geophys. Res.* **86**, 9776.

Wang Q.-L., Chetelat B., Zhao Z.-Q., Ding H., Li S.-L., Wang B.-L., Li J. and Liu X.-L. (2015) Behavior of lithium isotopes in the Changjiang River system: Sources effects and response to weathering and erosion. *Geochim. Cosmochim. Acta* **151**, 117–132.

West A. J., Galy A. and Bickle M. (2005) Tectonic and climatic controls on silicate weathering. *Earth Planet. Sci. Lett.* **235**, 211–228.

Weynell M., Wiechert U. and Schuessler J. A. (2017) Lithium isotopes and implications on chemical weathering in the catchment of Lake Donggi Cona, northeastern Tibetan Plateau. *Geochim. Cosmochim. Acta* **213**, 155–177.

Wimpenny J., Colla C. A., Yu P., Yin Q. Z., Rustad J. R. and Casey W. H. (2015) Lithium isotope fractionation during uptake by gibbsite. *Geochim. Cosmochim. Acta* **168**.

Wimpenny J., Gisalason S.R., James R.H., Gannoun A., Pogge von Strandmann P.A.E., Burton K.W. (2010a) The behaviour of Li and Mg isotopes during primary phase dissolution and secondary mineral formation in basalt. *Geochim. Cosmochim. Acta* **74**, 5259–5279.

Wimpenny J., James R. H., Burton K. W., Gannoun A., Mokadem F. and Gíslason S. R. (2010b) Glacial effects on weathering processes: New insights from the elemental and lithium isotopic composition of West Greenland rivers. *Earth Planet. Sci. Lett.* **290**, 427–437.

Witherow R. A., Lyons W. B. and Henderson G. M. (2010) Lithium isotopic composition of the McMurdo Dry Valleys aquatic systems. *Chem. Geol.* **275**, 139–147.

Woo, M. K. (2012). Permafrost hydrology. Springer Science & Business Media.

Yang, D., Kane, D., Hinzman, L., Zhang, X., Zhang, T. & Ye, H. 2002. Siberian Lena river hydrologic regime and recent change. *J. Geophys. Res.* **107**(D23): 4694.

Ye B., Yang D. and Kane D. L. (2003) Changes in Lena River streamflow hydrology: Human impacts versus natural variations. *Water Resour. Res.* **39**.

Yoon J. (2010) Lithium as a Silicate Weathering Proxy: Problems and Perspectives. *Aquat. Geochemistry* **16**, 189–206.

Zhang L., Chan L.-H. and Gieskes J. M. (1998) Lithium isotope geochemistry of pore waters from ocean drilling program Sites 918 and 919, Irminger Basin. *Geochim. Cosmochim. Acta* **62**, 2437–2450.

881 **Figures**

882

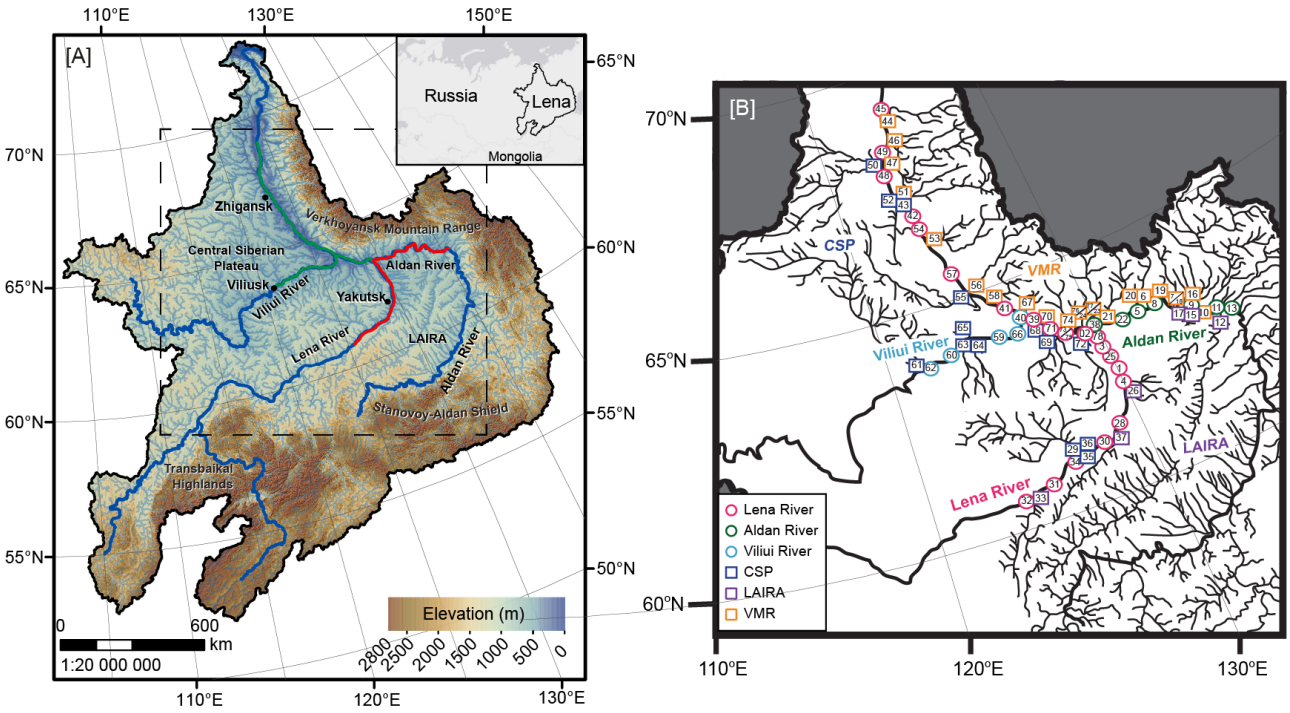

883

884 Figure 1: Map showing the Lena River catchment and its sub-catchment regions with the July 2012
885 sampling route shown in red and June 2013 in green in panel A. In panel B, sampling locations are
886 shown, with those within the Lena River main channel or the Viliui and Aldan Rivers, which are major
887 tributaries, denoted by circles. Smaller tributaries of the Central Siberian Plateau (CSP), Lena-
888 Amginsky inter-river area (LAIRA) and Verkhoyansk Mountain Range (VMR) are denoted by squares
889 (maps modified after Hirst et al. 2017). The same symbols and colour scheme are used in subsequent
890 figures.

891

892

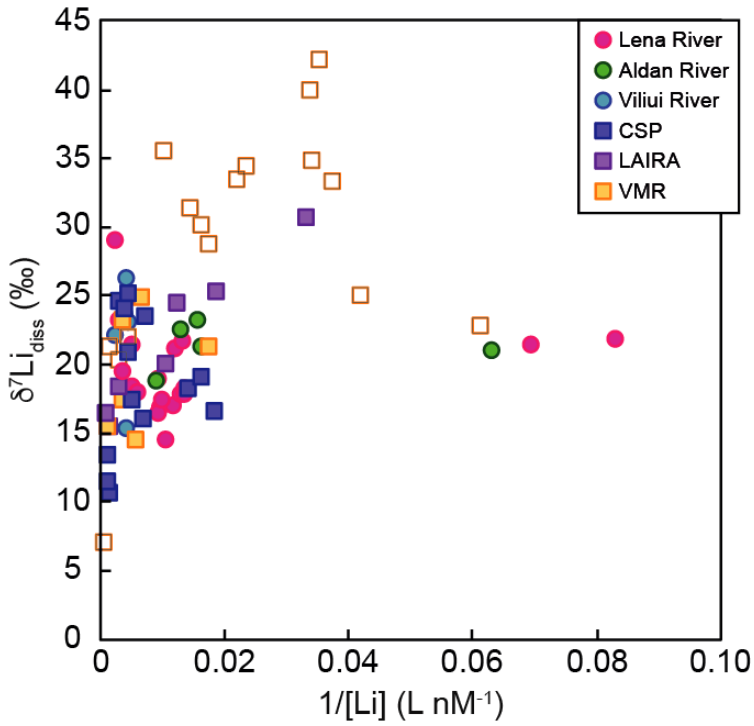

Figure 2: δ^7Li_{diss} compositions and dissolved Li concentrations for rivers in the Lena River watershed, with previous values from the watershed (Huh et al., 1998a) shown for comparison (not shown is one anomalous sample UL436 that drains the evaporitic marine carbonates within the Siberian Platform with high [Li] of 3350 nM and δ^7Li_{diss} = 21.2‰). Uncertainties on δ^7Li smaller than the symbols. CSP = Central Siberian Plateau; LAIRA = Lena-Amginsky inter-river area; VMR = Verkhoyansk Mountain Range. Open symbols represent VMR rivers draining south-facing catchments, which show the greatest variation in both [Li] and δ^7Li_{diss}.

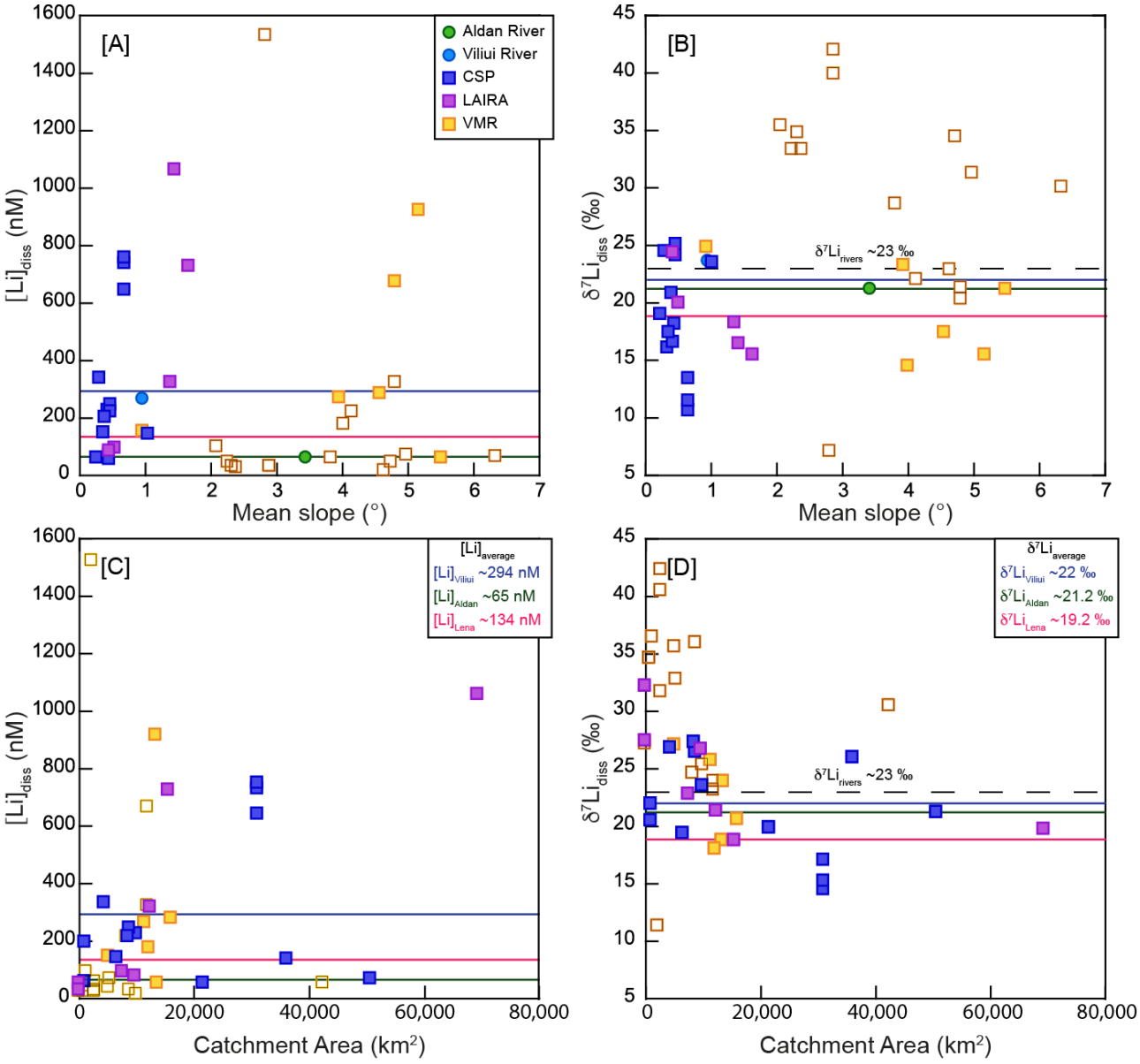

Figure 3: Dissolved Li concentrations and δ^7Li compositions compared with watershed gradient [A,B] and catchment area [C,D] for tributaries draining into the Lena, Viliui and Aldan Rivers. CSP = Central Siberian Plateau; LAIRA = Lena-Amginsky inter-river area; VMR = Verkhoyansk Mountain Range.

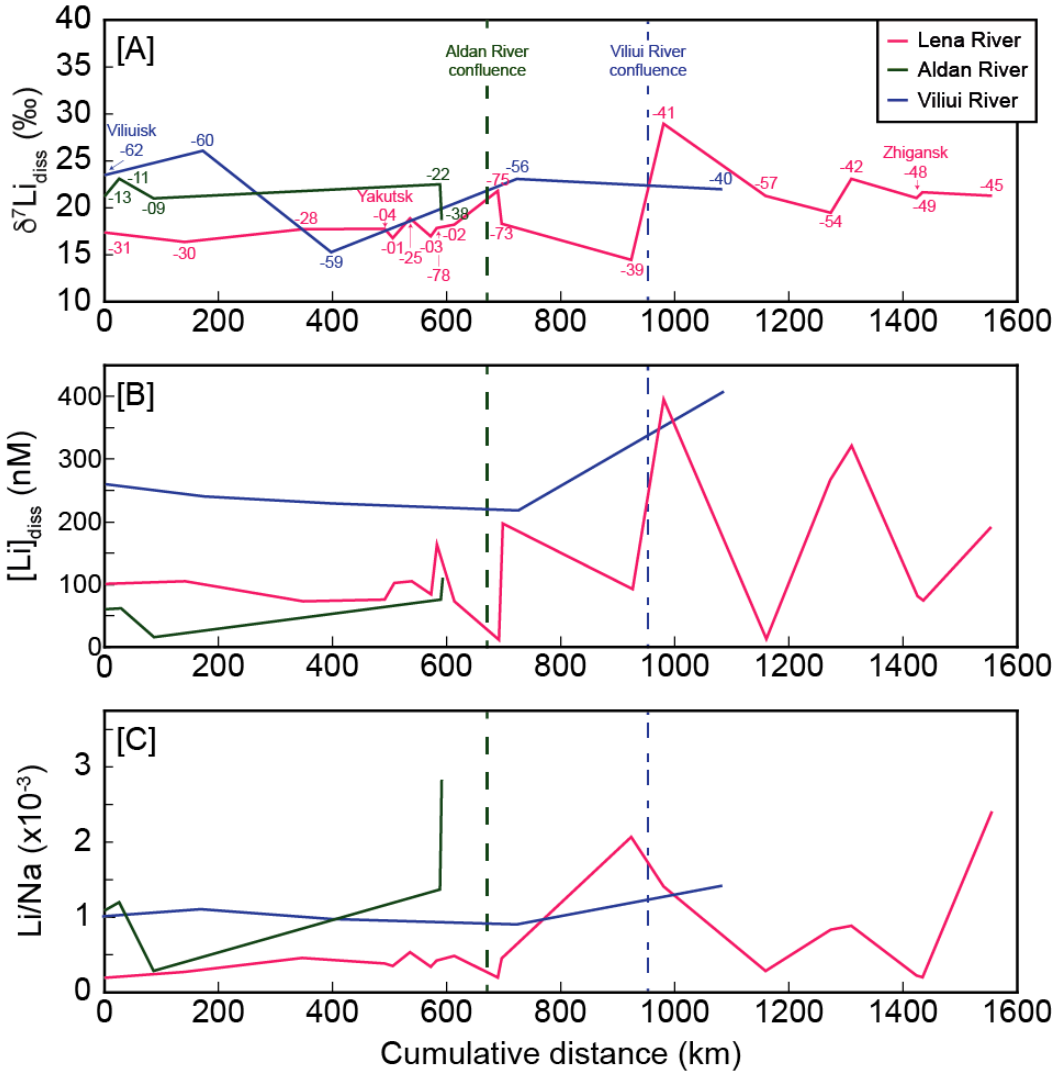

Figure 4: Downstream variations in δ^7Li_{diss}, [Li] and Li/Na in the Lena River main channel, and major tributaries of the Aldan and Viliui Rivers that converge into the main channel. River samples numbers are shown adjacent to curves, and arrows indicate the downstream river location of major towns. Confluences of the Aldan and Viliui Rivers into the Lena River main channel are shown as dashed lines. See Figure 1 for more information. No systematic trends can be observed in [Li], or Li/Na. A gradual ~5‰ increase can be seen along the Lena River main channel, see text for further details.

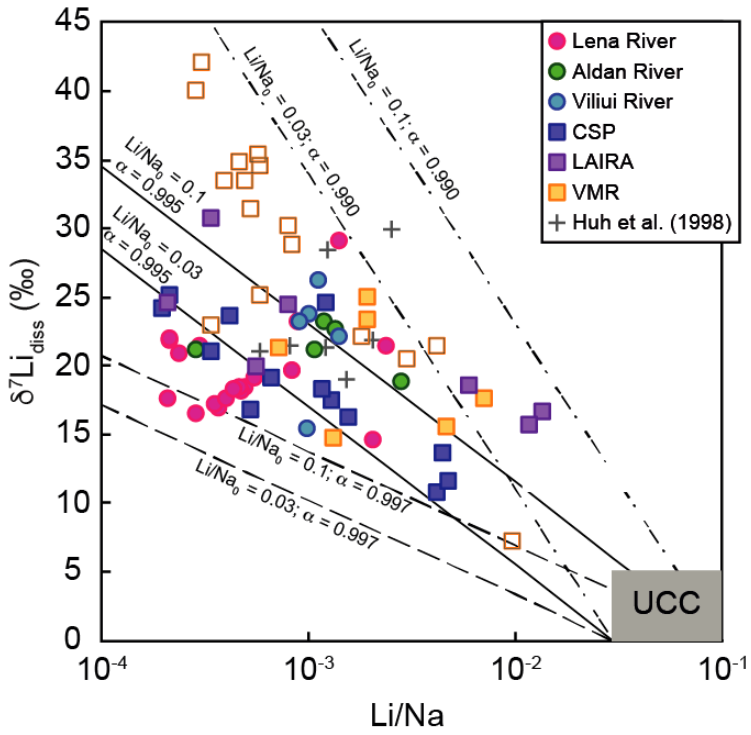

Figure 5: Relationship between measured δ^7Li_{diss} and Li/Na molar ratios for the Lena River. Shown for comparison are Lena River data from Huh et al. (1998). The lines represent the evolution of δ^7Li and Li/Na for a model in which Li is supplied to waters by dissolution of primary silicate minerals and this is followed by progressive removal of Li into secondary minerals. Curves are shown for different starting values and different fractionation factors for Li removal. The grey field represents the range of values that are generally expected for dissolution of silicate rocks, with Li/Na molar ratios between the highest measured in the Lena River watershed and the composition of UCC and δ^7Li values for the upper continental crust and typical shales (Taylor and McLennan, 1995; Teng et al., 2004; Dellinger et al., 2014; Sauzéat et al., 2015). CSP = Central Siberian Plateau; LAIRA = Lena-Amginsky inter-river area; VMR = Verkhoyansk Mountain Range. Open symbols represent VMR rivers draining south-facing catchments.

931

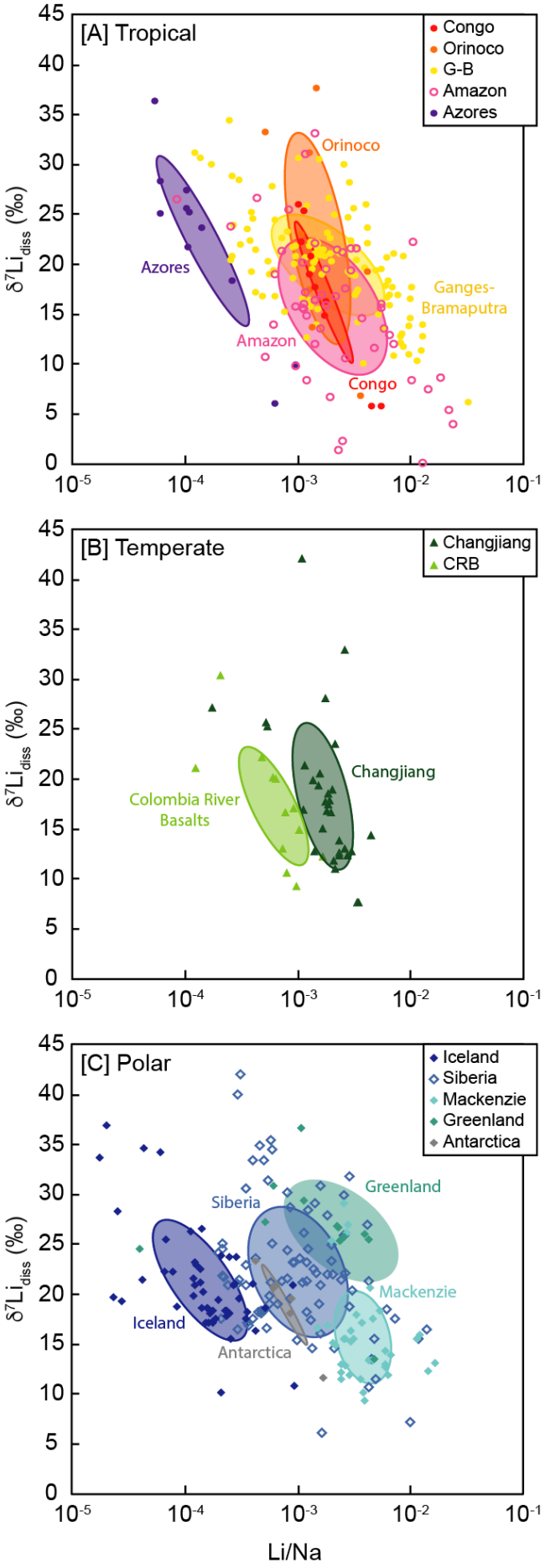
[A] Tropical
Congo
Orinoco
G-B
Amazon
Azores
Orinoco
Azores
Ganges-
Bramaputra
Amazon
Congo
[B] Temperate
Changjiang
CRB
Changjiang
Colombia River
Basalts
[C] Polar
Iceland
Siberia
Mackenzie
Greenland
Antarctica
Greenland
Siberia
Mackenzie
Iceland
Antarctica
δ7Lidiss (‰)
Li/Na
0
5
10
15
20
25
30
35
40
45
10-5
10-4
10-3
10-2
10-1

Figure 6: A compilation of dissolved Li isotope values versus molar Li/Na for rivers in [A] tropical, [B] temperate and [C] polar regions. Data include the Lena River and other Siberian rivers (this study; Huh et al., 1998a); the Mackenzie River (Millot et al., 2003; Millot et al., 2010); Antarctic rivers (Witherow et al., 2010); Greenland (Wimpenny et al., 2010b); the High Himalayas (Huh et al., 1998a; Kısakűrek et al., 2005); the Ganges-Brahmaputra (Huh et al., 1998a; Kısakűrek et al., 2005; Bagard et al., 2015; Frings et al., 2015; Manaka et al., 2017; Pogge von Strandmann et al., 2017); the Amazon (Huh et al., 1998a; Dellinger et al., 2015); the Orinoco (Stallard et al., 1995;1996; Huh et al., 1998a); the Congo (Henchiri et al., 2016); Changjiang (Yangtzee) River (Huh et al., 1998a; Liu et al., 2011; Wang et al., 2015); and basalts from Iceland, the Azores and the Columbia River Basalts (Pogge von Strandmann et al., 2006; Vigier et al., 2009; Pogge von Strandmann et al., 2010; Liu et al., 2015).

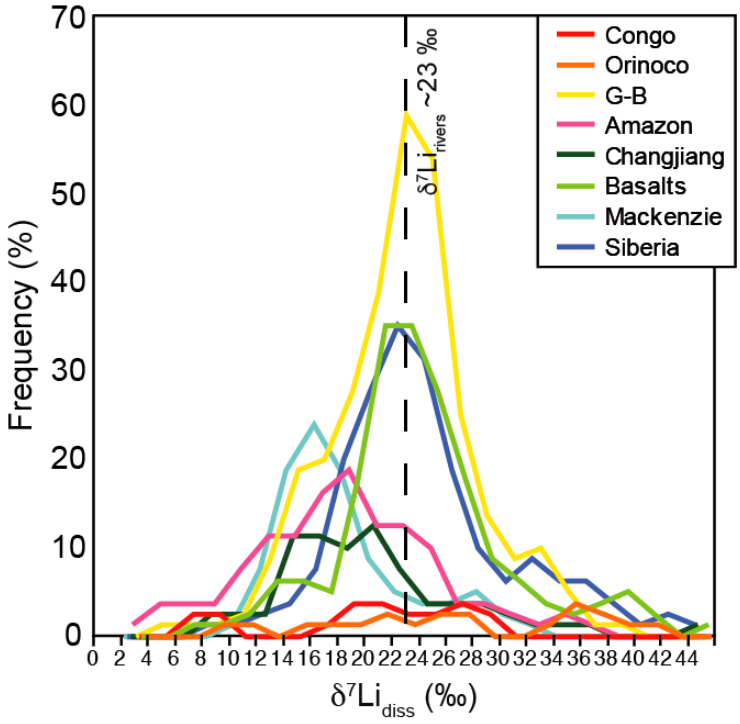

Figure 7: Histograms summarising dissolved δ^7Li compositions from large global rivers, and rivers draining basaltic terrains. A large peak can be seen clustering around the global median value of 23‰ (Huh et al., 1998b), with a smaller peak around ~14 to 16‰. Data from same sources as Fig. 6.